CrossMark

Viscous Evolution of Magnetized Clumps: A Source for X-Ray Flares in Gamma-Ray Bursts

Narjes Shahamat and Shahram Abbassi
Department of Physics, School of Science, Ferdowsi University of Mashhad, Mashhad, P.O. Box 91775-1436 Iran; n.shahamat.d@gmail.com, abbassi@um.ac.ir

Abstract

X-ray flares may indicate the late-time activity of the central engines of gamma-ray bursts. Such long-term activity has been described through some models, one of which is the viscous evolution of the outer disk's fragments proposed by Perna et al., and developed quantitatively by Dall'Osso et al. Here, we reconstruct the framework of Dall'Osso et al. by taking both small- and large-scale effects of magnetic field into account. To consider the magnetic barrier as a possible mechanism that might govern the accretion process of each magnetized clump, we construct a simple pattern in boundary conditions through which this mechanism might act. Regarding various model parameters, we probe for their influence and follow some key analogies between our model predictions and previous phenomenological estimates, for two different choices of boundary conditions (with and without a magnetic barrier). Our model is remarkably capable of matching the bolometric and X-ray light curves of flares, as well as reproducing their statistical properties, such as the ratios between rise and decay time, width parameter and peak time, and the power-law correlation between peak luminosity and peak time. Combining our results with the conclusions of previous studies, we are led to interpret a magnetic barrier as a less probable mechanism that might control the evolution of these clumps, especially those created later (or viscously evolved ones).

Unified Astronomy Thesaurus concepts: Accretion (14); Gamma-ray bursts (629); Magnetic fields (994)

1. Introduction

X-ray flares are detected in about one third of *Swift* gamma-ray bursts (GRBs) (Burrows et al. 2005; Falcone et al. 2006; Nousek et al. 2006; Zhang et al. 2006), and marked as one of the most common phenomena that reveal the late-time erratic behavior of GRBs' central engines. Flares are detected in both long and short GRBs (Campana et al. 2006; Falcone et al. 2006; Romano et al. 2006; Margutti et al. 2011), and appear mostly in a time window of 10^2–10^5 s (Chincarini et al. 2010; Yi et al. 2016), which overlaps the afterglow timescale.

Several models have been proposed over the years to describe this late-time flaring activity. The leading external shock scenario (e.g., Meszaros & Rees 1997) failed to justify the temporal properties of X-ray flares. In particular, Lazzati & Perna (2007) argued that inhomogeneities in the external shock prevent this model from reproducing the observational properties of the flares. On the other hand, making more detailed analogies between the temporal and spectral properties of the flares and those of prompt emissions (e.g., Margutti et al. 2010) favors the idea that flares and prompt pulses have a common origin, that is to say they both trace the activity of the central engine (for more discussions see, e.g., Ioka et al. 2005; Beniamini & Kumar 2016). Therefore, studying the origin of the flares might open a new window on GRBs' central engines.

A variety of efforts have been made to attribute the flares to evolution of the central engine. King et al. (2005) suggested that fragmentation of a collapsing star and its subsequent accretion can lead to X-ray flare production. Moreover, ring-like fragmentation of the outer regions in a hyperaccreting disk might cause such a flaring activity, as proposed by Perna et al. (2006). From the magnetic point of view, some scenarios have been proposed that support the long-term activity of the central engine, e.g., late-time episodic accretion caused by a magnetic flux accumulation in the inner disk regimes, i.e., a magnetic barrier (Proga & Zhang 2006), and magnetic reconnection in a differentially rotating millisecond pulsar (Dai et al. 2006).

Motivated by the observed correlation between a flare's duration and its arrival time (Cusumano et al. 2006; O'Brien et al. 2006), and the similarity in the distributions of waiting times of X-ray flares and prompt gamma-ray emissions, which might lead to the consideration of a similar physical source for both events (Guidorzi et al. 2015), Dall'Osso et al. (2017) developed the idea of disk fragmentation in a more quantitative manner. They suggest that various flares with different arrival times (including both early and late-time ones) might be attributed to the viscous spreading of different clumps created during the early or late-time phase of central engine evolution. More specifically, they introduced an offset time as the time delay between the GRB trigger and the time at which X-ray flares set in, and argued that different offset times are subject to the starting point of various clumps' viscous evolution. So the early flares are considered to be caused by the prompt accretion of clumps generated during the early activity phase, while the delayed flares are due to clumps accreted later, or to fragments generated early that need to migrate toward the inner regions in order for viscous stress to dominate. They then provided a semi-analytical solution to this viscously evolved clump, and reproduced light curves of X-ray flares that, interestingly, matched the data well, after implementing some spectral corrections.

On the other hand, Shahamat & Abbassi (2017) studied the effects of magnetic field on both the vertical structure and neutrino luminosity of a self-gravitating neutrino-dominated accretion disk, as a plausible candidate for early-phase activity of GRB's central engine. The strongly magnetized nature of the disk, with a magnetic field of about 10^{15-16} G, made both small- and large-scale effects of the magnetic field worth studying (the former was studied through magnetic viscosity, the latter via the magnetic braking process). They mainly found

that such a consideration may shrink the gravitationally unstable regions toward the outer initial disk, and they highlight a magnetic barrier as a plausible mechanism for the lower accretion rates. All these findings, together with the fact that GRBs' central engines are supposed to be highly magnetized, lead us to develop the scenario of Dall'Osso et al. (2017) through taking the effects of magnetic field (small and large scale) into account, and to probe how the combination of magnetic barrier and fragmentation might affect this intriguing model to describe the light curves of X-ray flares.

Different approaches in the literature have addressed the magnetic barrier mechanism. For instance, D'Angelo & Spruit (2010, 2011, 2012) studied a magnetically truncated disk around a star (such as a neutron star). As they pointed out, the strong magnetic field near the star truncates the accretion disk. Due to angular momentum transfer between magnetic field and disk, one plausible state is that the disk is truncated outside the corotation radius $R_c = (GM_*/\Omega_*^2)^{1/3}$ (at which the frequency of the star's rotation equals the Keplerian frequency), where M_* and Ω_* are the mass and rotational frequency of the star. In this case a centrifugal barrier prevents the disk from accreting. Furthermore, the magnetic field lines form a "propeller regime." Such a topology of the field lines causes the gas inside the magnetospheric radius, R_m (the radius at which the accumulated magnetic field disrupts the accretion flow), to flow in freely along field lines toward the star's magnetic poles (Narayan et al. 2003). On the other hand, Narayan et al. (2003) discussed the physical conditions that govern the magnetically arrested disks (MADs) around black holes. They argue that MADs are considered to be accreting structures that are disrupted at R_m by the accumulated poloidal magnetic field in the vicinity of black holes. For $R > R_m$ the flow is axisymmetric, while for $R < R_m$ the flow breaks up into blobs or streams. Such streams or blobs can flow in slowly (with a velocity much less than the freefall velocity) toward the black hole via magnetic interchanges and reconnection. Regarding physical conditions imposed by a magnetic barrier around black holes, we adopt the strategy of Narayan et al. (2003), which leads us to consider two limiting boundary conditions. The first one is zero mass flux rate at the inner radius, and the second is taking the magnetospheric radius (R_m) as the inner boundary of the disk, namely $R_{\rm in}$.

In the present paper, Section 2 manifests our model framework with a clarification of all the assumptions and approximations we made in order to smooth our way in extracting a semi-analytical solution, following the approach of Dall'Osso et al. (2017). The correlation between our model parameters and those related to the shape of the light curve will be considered in Section 3, together with some key analogies between our model predictions and observations. We then summarize and discuss our main conclusions in Section 4.

2. Ring-like Fragments and Their Viscous Evolution

Hyperaccreting disks are gravitationally unstable in their outer regions, which might result in disk fragmentation and be a source of a disk's late-time activity (i.e., X-ray flares), as suggested by Perna et al. (2006), and discussed by Liu et al. (2014) and Shahamat & Abbassi (2017). A disk becomes gravitationally unstable once the Toomre parameter, Q, satisfies

(Toomre 1964)

$$Q = \frac{c_s \Omega}{\pi G \Sigma} < 1 \qquad (1)$$

where c_s is the sound speed, Ω is the local Keplerian angular velocity, G is the gravitational constant, and Σ is the disk surface density. In the magnetized case, this criterion takes the form (Shu 1992)

$$Q_{\rm mag} = \frac{\sqrt{c_s^2 + v_A^2}\,\Omega}{\pi \Sigma G} < 1 \qquad (2)$$

where $v_A = \frac{B}{\sqrt{4\pi\rho}}$ is the Alfvén velocity. However, in these unstable regimes, fragmentation into bound objects will occur if (Gammie 2001; Perna et al. 2006)

$$t_{\rm cool} < t_{\rm cirt} \approx 3\Omega^{-1}, \qquad (3)$$

where the cooling timescale is denoted by $t_{\rm cool} \approx (H/R)^2 t_\nu$ (Pringle 1991), with $t_\nu = \frac{2}{3}\frac{R^2}{\nu}$ regarded as the viscous timescale and $t_{\rm cirt}$ is the critical time scale. Fragments merge and/or accrete until their tidal influence gets strong enough to open a gap in the disk. This happens when the mass of the clump has increased to

$$M_{\rm frag} \simeq \left(\frac{H}{R}\right)^2 \alpha^{1/2} M_{\rm BH}. \qquad (4)$$

where $M_{\rm BH}$ is the mass of the central black hole (Takeuchi et al. 1996; Dall'Osso et al. 2017), H is the half thickness of the disk, and α is the viscous parameter.

In what follows, regarding the model proposed by Perna et al. (2006), we suppose that such a ring-like clump has been created in the outer regions as a sharp accumulated mass, more specifically a delta function, at radius R_0. Computing the viscous evolution of the clump, we also consider the standard equation for axisymmetric accretion disks (Kato et al. 2008):

$$\frac{\partial}{\partial t}\Sigma(R, t) = \frac{1}{R}\frac{\partial}{\partial R}\left(R^{1/2}\frac{\partial}{\partial R}(3\nu\Sigma R^{1/2})\right). \qquad (5)$$

Although this equation seems to ignore magnetic field effects, the small-scale effect of magnetic field can be taken into account through the magnetic viscosity term, i.e., ν. Hence, being interested in considering the large-scale effect of magnetic field, we add a term corresponding to the torque exerted by the Lorentz force. To do so, we make use of the approach of Lee et al. (2000) and Shahamat & Abbassi (2017) to modify Equation (5) to

$$\frac{\partial}{\partial t}\Sigma(R, t) = -\frac{1}{R}\frac{\partial}{\partial R}\left[\frac{\frac{\partial}{\partial R}\left(R^3\nu\Sigma\frac{d\Omega}{dr}\right) + \frac{R^2 B_\phi B_z}{2\pi}}{\frac{d}{dR}(R^2\Omega)}\right]. \qquad (6)$$

Considering the common assumption $B_z \approx B_R$ (e.g., Proga & Zhang 2006; Shahamat & Abbassi 2017), in order to get rid of the magnetic field components in the second term of the numerator, we can make use of the magnetic viscosity equation

$$\frac{B_R B_\phi}{4\pi} = -\frac{3}{2}\alpha P, \qquad (7)$$

where P is the total pressure of the accretion flow. On the other hand, we know that

$$P = -\frac{1}{\alpha}\rho\nu R\frac{d\Omega}{dR}, \tag{8}$$

and we consider $H\rho \approx \Sigma$ as a vertically averaged approximation (Kato et al. 2008). Finally, one can rewrite Equation (6) as

$$\frac{\partial}{\partial t}\Sigma(R, t) = -\frac{1}{R}\frac{\partial}{\partial R}\left[\frac{\frac{\partial}{\partial R}\left(R^3\nu\Sigma\frac{d\Omega}{dr}\right) + 3\frac{d\Omega}{dR}\frac{\Sigma}{h}\nu R^2}{\frac{d}{dR}(R^2\Omega)}\right], \tag{9}$$

where $h = \frac{H}{R}$.

In general, the viscosity ν depends on the surface density and Equation (9) is nonlinear. If, however, ν is only a function of radius, then the equation is linear and much more amenable to analytic methods. Therefore, following Dall'Osso et al. (2017) and Tanaka (2011), we assume the viscosity to follow a radial power law, $\nu \propto R^n$, to achieve an exact solution for $\Sigma(R, t)$ using a Green's function G,

$$\Sigma(R, t) = \int_{R_{in}}^{\infty} G(R, R', t)\Sigma(R', t = 0)\, dR', \tag{10}$$

in which $\Sigma(R, t = 0)$ is a given arbitrary profile at $t = 0$. Having $\Sigma(R, t)$, the accretion power L_{acc}, due to the viscous spreading of the clump, is approximately

$$L_{acc} \simeq \int_{R_{in}}^{\infty} \frac{9}{4}\Sigma(R, t)\nu(R)\Omega^2(R)2\pi R\, dR. \tag{11}$$

To compute the Green's function, we need to determine our desired boundary condition. In this regard, we encounter two strategies. The first is a boundary condition of zero central torque, which is of astrophysical interest especially in the case of accretion onto a black hole or a slowly rotating star, at radii larger than the radius of the innermost circular orbit or the stellar surface, respectively. The other is a boundary condition of zero mass flux. Having a strong central source of angular momentum, the accreting gas will be prevented from flowing in, and will instead accumulate near the center (Tanaka 2011). Such solutions can describe accretion disks around a compact binary (Pringle 1991), and also compact objects with strong central magnetic fields (Lynden-Bell & Pringle 1974). The latter seems similar to the physical situation imposed by the accumulated poloidal magnetic field near the innermost region of MADs, which might result in a magnetic barrier mechanism (Narayan et al. 2003; Shahamat & Abbassi 2017). Therefore, we are to apply both boundary conditions, in order to probe the effect of a magnetic barrier on the light curve of an X-ray flare.

Obtaining the appropriate Green's function, in the case of a boundary condition of zero torque, the surface density integral takes the following form:

$$\frac{\Sigma}{\Sigma_0} = \int_0^{\infty} \frac{R}{R_0}^{-n+(1-b_1)/2}\left(\frac{R_0}{R_{in}}\right)^{2-n}$$
$$\times (1 - n/2)e^{-2\kappa^2(1-n/2)^2 t/t_{\nu_{in}}}$$
$$\times [Y_l(\kappa)J_l(\kappa x_0) - Y_l(\kappa x_0)J_l(\kappa)]$$
$$\times \frac{[Y_l(\kappa)J_l(\kappa x) - Y_l(\kappa x)J_l(\kappa)]}{[Y_l^2(\kappa) + J_l^2(\kappa)]}\kappa\, d\kappa \tag{12}$$

and in the case of a boundary condition of zero mass flux one may achieve

$$\frac{\Sigma}{\Sigma_0} = \int_0^{\infty} \frac{R}{R_0}^{-n+(1-b_1)/2}\left(\frac{R_0}{R_{in}}\right)^{2-n}$$
$$\times (1 - n/2)e^{-2\kappa^2(1-n/2)^2 t/t_{\nu_{in}}}$$
$$\times [Y_{l-1}(\kappa)J_l(\kappa x_0) - Y_l(\kappa x_0)J_{l-1}(\kappa)]$$
$$\times \frac{Y_{l-1}(\kappa)J_l(\kappa x) - Y_l(\kappa x)J_{l-1}(\kappa)}{Y_{l-1}^2(\kappa) + J_{l-1}^2(\kappa)}\kappa\, d\kappa. \tag{13}$$

To learn about new parameters and variables, and to get an insight into the adopted procedure, we refer readers to the Appendix.

What matters right now is how to fix the parameters Σ_0 and R_0.

2.1. Determination of Σ_0 and R_0

As previously stated, one can assume the ring-like clump to be a sharp concentration at radius R_0. This radius can be regarded as the same as that of gravitational instability. Therefore, we approximated Σ_0 with the expression

$$\Sigma_0 \simeq \frac{M_{frag}}{2\pi R_0 l_{cl}} \approx \frac{M_{frag}}{2\pi R_{ins} l_{cl}} \tag{14}$$

where l_{cl} denotes the clump size, which can be estimated as the local Jeans length (λ_j). First, to evaluate R_0, we need to find an expression for R_{ins}. This can be fulfilled by the use of the Toomre criterion (Equation (2)). Through some mathematical considerations as performed by Shahamat & Abbassi (2017), we can approximate magnetic pressure ($B^2/8\pi$) with the total pressure (P). Mathematically speaking, one knows that

$$B^2/8\pi < P + B^2/8\pi,$$

we then have

$$p_{mag} \approx \beta(P + B^2/8\pi) \quad \text{with } \beta < 1.$$

This provides us with the following expression:

$$B^2 = 8\pi\frac{\beta}{1-\beta}P \approx 0.3P \tag{15}$$

in which, to get the last equality, we choose β to be 0.01, which is the same value as adopted by Shahamat & Abbassi (2017). With the help of Equation (8) we reach

$$B^2 = -\frac{0.3}{\alpha}\rho\nu R\frac{d\Omega}{dR}. \tag{16}$$

Replacing these quantities, and applying relations $\dot{M} = 3\pi\Sigma\nu$ (valid for steady accretion) and $n = 1/2$ (an acceptable value for advection-dominated disks, see, e.g., Tanaka 2013), one may obtain

$$R > \left(3h^2\alpha\frac{M}{\dot{M}}\sqrt{1.03h^2 GM}\right)^{2/3} = R_{ins}. \tag{17}$$

Finally, we are in need of the local magnetic Jeans length, λ_{jmag}, which takes the form

$$\lambda_{jmag} = \lambda_j\sqrt{1 + \frac{v_A^2}{c_s^2}} = c_s\sqrt{\frac{\pi}{G\rho}}\sqrt{1 + \frac{v_A^2}{c_s^2}}. \tag{18}$$

3

Regarding all the above considerations, we will have

$$\lambda_{\text{jmag}} = \sqrt{\frac{3.1 h^5 \pi^2 \alpha M \sqrt{GM R_{\text{ins}}}}{\dot{M}}}. \qquad (19)$$

Hereby, we have our approximately estimated values for Σ_0 and R_0.

2.2. What about R_{in} and R_{out}?

The inner radius (R_{in}) differs in for the two different boundary conditions we adopted here. In the case of zero torque, we choose it to be equal to the innermost stable circular orbit, while for zero mass flux, in which the magnetic barrier can be taken into account, we considered the magnetospheric radius as the inner radius. This quantity can be defined as (Proga & Zhang 2006)

$$R_m \approx 60 \epsilon_{-3}^{2/3} \dot{M}_1^{-2/3} M_3^{-4/3} \phi_{30}^{4/3} \qquad (20)$$

where $\phi_{30} \equiv \phi/(10^{30} \, \text{cm}^2 \, \text{G})$. Here ϕ is the magnetic flux accumulated in the disk inner side and it has been taken to be about 10^{-2}, which can be supposed to be a typical value for the activity of the GRB's central engine (Xie et al. 2009; Shahamat & Abbassi 2017). Also, $\epsilon_{-3} = 10^3 \epsilon$, in which ϵ is a parameter defined to be the ratio of the radial velocity of the accreted matter to its freefall velocity inside the magnetospheric radius (Shahamat & Abbassi 2017). We adopted a value of 10^{-3} for ϵ. Indeed, this parameter is less certain (for more discussion about this parameter see, e.g., Lloyd-Ronning et al. 2016; Narayan et al. 2003). $\dot{M}_1$ and M_3 denote $\dot{M}/1 \, M_\odot \, \text{s}^{-1}$ and $M_{\text{BH}}/3 \, M_\odot$, respectively.

On the other hand, as time passes, the accretion rate declines after the prompt phase. Metzger et al. (2008) reported that a neutrino-cooled accretion disk, in its late-time viscous evolution, experiences a decreasing mass accretion rate with a self-similar behavior $\dot{M} \propto t^{-4/3}$. Hence, we approximate the late-time accretion rate as

$$\dot{M} = \dot{M}_0 \left(\frac{t}{t_0}\right)^{-4/3} \qquad (21)$$

where $\dot{M}_0$ is the accretion rate related to a given time, t_0, specified (arbitrarily) during the late activity phase. We have fixed $\dot{M}_0$ to have the value $0.04 \, M_\odot \, \text{s}^{-1}$ at $t_0 = 50 \, \text{s}$ after the prompt phase (which is supposed to have an accretion rate of about 0.1–$10 \, M_\odot \, \text{s}^{-1}$, typically).

In the context of the outer boundary, we consider R_{out} as the radius at which the viscous evolution of the clump sets in. To estimate this radius, we take the shear, self-gravity, and tidal forces per unit mass exerted on the clump as introduced by Dall'Osso et al. (2017). We then add the Lorentz force in order to account for the large-scale effects of magnetic field.

A clump of linear size l_{cl} and mass M_{cl} will be affected by the shear force per unit mass

$$F_\nu = \frac{l_{\text{cl}} \dot{M} \Omega}{2\pi M_{\text{cl}}} \qquad (22)$$

in which the relation $\dot{M} = 3\pi \nu \Sigma$, valid for a steady-state disk, has been considered.

Given the self-gravity force per unit mass of the clump, $F_{\text{SG}} = \frac{GM_{\text{cl}}}{l_{\text{cl}}^2}$, the tidal force due to the central object,

$F_T = \frac{GM_{\text{BH}}}{r^2}\left(\frac{l_{\text{cl}}}{r}\right)$ (Dall'Osso et al. 2017), and the Lorenz force per unit mass, $F_B = \frac{B_r B_\phi}{4\pi\Sigma}$ (Lee et al. 2000), viscous spreading of the clump will start roughly when $F_\nu + F_T + F_B > F_{\text{SG}}$. It is worth noting that, making use of Equation (7) and $\dot{M} = 3\pi\Sigma\nu$, the Lorentz force can be rewritten in the form $-\frac{9GM\alpha h}{4r^2}$. After all, the condition for being viscously evolved reads

$$\frac{GM l_{\text{cl}}}{r^3} + \frac{l_{\text{cl}} \dot{M}}{2\pi M_{\text{cl}}} \sqrt{\frac{GM}{r^3}} - \frac{9GM\alpha h}{4r^2} - \frac{GM_{\text{cl}}}{l_{\text{cl}}^2} > 0. \qquad (23)$$

The solution to this inequality can provide us with an upper limit for the outer boundary R_{out}.

2.3. Issues on Bolometric and X-Ray Luminosities

There are some significant points to be noted. It is the relativistic jet (which can be created through the Blandford–Znajek mechanism, as the most viable scenario that can efficiently extract the rotational energy of a spinning black hole by a large-scale magnetic field threading the disk (Blandford & Znajek 1977)) that might produce the GRB's X-ray flares. To be more precise, such emissions are subject to the radiative mechanisms through which the jet power is converted into radiation. For the sake of simplicity, we assume the radiative efficiency in the jet to be constant. Therefore, the bolometric luminosity of the flare will be

$$L_{\text{bol}} = f_{\text{rad}} L_{\text{acc}} \qquad (24)$$

where f_{rad} is the efficiency of conversion of energy from mass accretion into radiation, which we assume to be constant. We also adopted $f_{\text{rad}} \approx 0.5$ in view of discussions by Fragile et al. (2012). However, in case of the zero-flux boundary condition, i.e., taking the magnetic barrier into account, and consequently using the radiation efficiency in the MAD model (Narayan et al. 2003), we adopted a value of ~ 1.0 for f_{rad}, based on discussions by Tchekhovskoy et al. (2011) and McKinney et al. (2012).

On the other hand, we need to consider the X-ray bandpass (0.3–10 keV) in order to evaluate this model by making a comparison with observations that are performed in a finite X-ray energy band. Thus, an efficiency coefficient is required to consider the X-ray energy band instead of the bolometric light curve. Here, we follow Jin et al. (2010) and Fan & Piran (2006) by approximating the X-ray flare luminosity as a constant coefficient of bolometric luminosity, $L_X = f_X L_{\text{bol}}$, where f_X (X-ray flare efficiency) is estimated as ≈ 0.1.

3. Results

3.1. Correlation of Model Parameters and Spectral Properties

Our model contains some parameters, M_{BH}, h, and α, whose effects on shape parameters should be noticed. We introduce two shape parameters: k is the "asymmetry parameter," and w is the ratio of the width, $\Delta t = t_2 - t_1$, to the peak time, t_p. t_p is the time at which the peak luminosity L_p is expected. t_1 and t_2 refer to the times with fluxes of around L_p/e (the former during the rise and the latter during the decay). The asymmetry parameter is regarded as the ratio t_d/t_r, with rise time $t_r = t_p - t_1$ and decay time $t_d = t_2 - t_p$.

To gain an insight into how model parameters affect those related to the shape of the light curve, we provide some data, predicted by our model, in Table 1. It should be mentioned that

Table 1
Spectral and Model Parameters for the Boundary Conditions of Zero Torque and Zero Mass Flux

M_{BH} ($M_\odot$)	t_{off} (s)	h	α	M_{cl} ($M_\odot$)	t_p (s)	L_p (10^{48} erg s^{-1})	Δt (s)	w	k
10	100.0	0.6	0.01	0.36	110.0	1.4	16.0	0.15	2.5
10	200.0	0.6	0.01	0.36	220.5	0.6	32.0	0.15	2.3
10	100.0	0.5	0.01	0.25	105.0	1.6	7.5	0.07	2.7
10	200.0	0.5	0.01	0.25	210.5	0.7	15.0	0.07	2.0
5	50.0	0.9	0.01	0.4	61.5	2.12	21.5	0.3	2.5
5	100.0	0.9	0.01	0.4	122.5	0.73	43.0	0.3	2.7
3	50.0	0.9	0.01	0.2	57.0	2.1	12.5	0.2	2.51
3	100.0	0.9	0.01	0.2	113.5	0.7	26.0	0.22	2.7
3	50.0	0.9	0.1	0.76	57.0	2.7	12.5	0.2	2.5
3	100.0	0.9	0.1	0.76	114.5	1.15	26.5	0.23	2.7
2.5	1000.0	0.6	0.01	0.09	1094.5	0.023	148.0	0.14	2.4
2.5	1000.0	0.5	0.01	0.06	1048.5	0.03	69.0	0.07	2.2
2.5[a]	200.0	0.8	0.15	0.6	215.0	6.0	26.0	0.12	2.7
2.5[a]	300.0	0.8	0.15	0.6	340.5	1.12	70.5	0.2	2.7
3[a]	200.0	0.8	0.13	0.7	218.0	8.0	31.5	0.15	2.7
3[a]	300.0	0.8	0.13	0.7	349.0	1.5	85.0	0.24	2.6

Note.
[a] Cases with zero-flux boundary condition.

we considered $0.5 \leqslant h \leqslant 1$ (valid for the late-time advection-dominated phase of the GRB's central engine, e.g., Metzger et al. 2008), and $0.01 \leqslant \alpha \leqslant 0.2$, which is a physically justified interval (e.g., McKinney et al. 2012). Generally speaking, we interestingly found that the shape parameters, w and k, are not significantly sensitive to the model parameters, regardless of some scatter. This fact that has been confirmed by the statistical analysis of observational data, and will be discussed in more detail in Section 3.2.

To elaborate how effective the model parameters are, we point to their impact on the clump mass, and subsequently on the maximum amount of flux and the width parameter, which might directly affect the shape of the light curve. First, as h grows, the clump mass increases, and this leads to a decline in the peak luminosity and an increase in the width parameter as well as peak time, i.e., the light curve gets wider with less maximum radiated flux. At first glance, this might appear to contradict the fact that the larger the clump mass is, the higher the total radiated energy gets ($E \propto M_{cl}$). For one thing, we found that the radius at which the viscous evolution is triggered is less for small h than for a thicker clump. For instance, R_0 (which is chosen to be the same as R_{ins}, since the viscous evolution constraint (23) is respected by this radius, in this case) is $905.2 R_g$ for the set of parameters $M_{BH} = 10$, $h = 0.5$, $\alpha = 0.01$, and $t_{off} = 200$ s, while it is about $1303.5 R_g$ in the similar case with $h = 0.6$. For another thing, the clump is denser in the former case than in the latter. Subsequently, the flare duration (which might be estimated to be of the order of the width parameter) will be considerably less for the thinner clump than for the thicker one, as one can see in data provided in Table 1. Thus, we are of the opinion that the heavier clump is expected to radiate more total energy, although its lower density located at a farther distance causes such a decline in the luminosity. On the other hand, this behavior can be explained through the explicit dependence of luminosity on h. Concerning Equation (4), clump mass increases in proportion to h^2. Also, R_0 ($\sim R_{ins}$) is proportional to h^2, as appears in Equation (17). These two proportionalities together with the relation between l_{cl} and h ($l_{cl}(\sim \lambda_{jmag}) \propto h^3$) cause Σ_0 to be proportional to h^{-3}, regarding

Equation (14). Thus, one may conclude that Σ has a reverse relation with h (i.e., $\Sigma \propto h^{-1.5(1+1/h)}$), and this subsequently leads the luminosity to drop as h grows, considering Equation (11). Apparently, this result opposes the outcome of Dall'Osso et al. (2017), because they conclude that for the same initial radius (R_0), a more massive clump produces a larger peak luminosity. Such an inconsistency stems from ignoring correlations that we considered between model parameters in our framework and fixing them arbitrarily.

Second, our data demonstrate that any increase in the α parameter might enhance the clump mass remarkably, while the width parameter might not be affected considerably, so that the peak luminosity grows. This fact has been also inferred by Dall'Osso et al. (2017). Finally, we came to the conclusion that growth of the black hole mass may lead to a heavier clump with a rather higher luminosity, which happens over a longer timescale. In this case, the growth of the clump mass is apparently more significant than the increase in duration, so that a final higher luminosity is produced.

Overall, such correlations between model parameters and spectral quantities are can be inferred from our data; however, in agreement with Dall'Osso et al. (2017) and observational analysis, the shape parameters w and k are not strongly affected by our model parameters, regardless of their somewhat scattered behavior.

3.2. Observations and Model Predictions

From the study by Chincarini et al. (2010) of 113 flares in the 0.3–10 keV energy band of the X-ray Telescope (XRT), and four subenergy bands, some observational characteristics of the X-ray light curves can be clarified as follows.

(i) The ratio of rise time to decay time is constant, implying that both timescales grow by the same factor, so that $t_d \approx 2t_r$. Consequently, flares are self-similar in time.

(ii) The width evolves linearly with the peak time: $w \approx 0.2$. These two points are the key features that strongly distinguish the flare emission from the prompt phase.
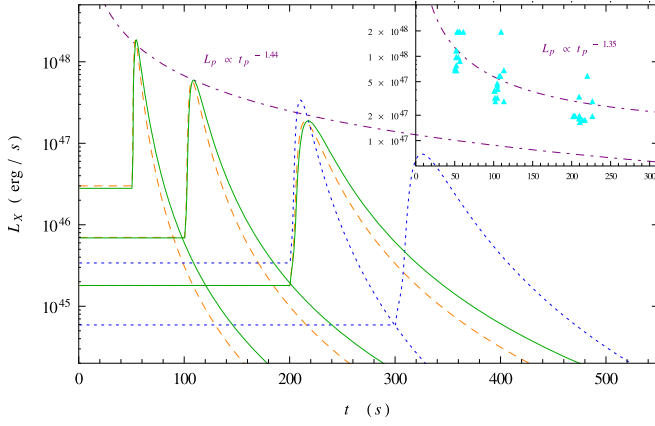
Figure 1. X-ray luminosity light curve for three sets of model parameters: $M_{\rm BH} = 3\,M_\odot$, $h = 0.8$, and $\alpha = 0.13$ (green curves), $M_{\rm BH} = 2.5\,M_\odot$, $h = 0.8$ and $\alpha = 0.15$ (orange dashed curves), and $M_{\rm BH} = 5\,M_\odot$, $h = 0.6$, and $\alpha = 0.22$ (blue dotted curves). The vertical axis is on a logarithmic scale. Four different offset times, $t_{\rm off} = 50$ s, 100 s, 200 s, and 300 s, are included in the case of a zero-torque boundary condition. The dotted–dashed lines in purple depict the best power-law fit for the peak luminosity and peak time, which are in good agreement with observations.

Moreover, analyzing 468 bright X-ray flares from the GRBs observed by *Swift* between 2005 and 2015, Yi et al. (2016) argued that the peak luminosity decreases with the peak time, following a power-law behavior $L_p \propto t_p^{-1.27}$.

In general, for both boundary conditions, our model leads to rather observationally well matched predictions, considering the mentioned shape parameters.

In the case of a zero-torque boundary condition, Figures 1 and 2 demonstrate how our model respects these three criteria. We have considered a variety of model parameters, specified within the panels, and different offset times during the early phase of flaring activity (with $t_p < 1000$ s), i.e., 50 s, 100 s, 200 s, and 1000 s, in order to enhance the validity of our fits.

Figure 1 reflects the logarithmic behavior of X-ray luminosity over time. Four different offset times of 50 s, 100 s, 200 s, and 300 s have been considered. The best fit for peak luminosity versus peak time (the purple dotted–dashed line) indicates a power-law trend with a power index of ~-1.44, which is interestingly close to the value discussed by Yi et al. (2016), i.e., -1.27. These light curves have been plotted for three sets of model parameters: $M_{\rm BH} = 3\,M_\odot$, $h = 0.8$, and $\alpha = 0.13$ (green curves), $M_{\rm BH} = 2.5\,M_\odot$, $h = 0.8$, and $\alpha = 0.15$ (orange dashed curves), and $M_{\rm BH} = 5\,M_\odot$, $h = 0.6$, and $\alpha = 0.22$ (blue dotted curves). The inset panel shows the fit for a broader range of model parameters including those considered in Figure 2. Being of a rather similar power index, i.e., ~-1.35, the variation of model parameters does not affect the correlation we obtained in our model, which is in good agreement with its phenomenological relation, namely $L_p \propto t_p^{-1.27}$. On the other hand, as expressed in Section 3.1, Figure 2 reveals the robustness of the shape of the light curve in our model through the considerable (acceptable) insensitivity of the asymmetry parameter (width over peak time). Furthermore, our predicted values for these two shape parameters, i.e., $k \approx 2.5$ and $w \approx 0.11$, are in rather good agreement with those predicted by Chincarini et al. (2010), i.e., $k \approx 2$ and $w \approx 0.2$.

In order to obtain results for the zero-mass-flux boundary condition, and consequently take the magnetic barrier into account, we need to probe for a set of model parameters that satisfy the condition

$$\tau = \frac{t_\nu}{t_{\rm diff}} < 1 \qquad (25)$$

where $t_{\rm diff} \approx H/v_{\rm A}$ is the diffusion timescale that estimates the magnetic field buoyancy and the time it takes to rise to the disk surface (Shahamat & Abbassi 2017). Such a limitation ensures that the magnetic barrier is likely to exist during the clump's accretion due to the accumulation of the magnetic flux inside the inner regions (Xie et al. 2009; Shahamat & Abbassi 2017). The adopted parameters in Figures 3 and 4 comply with this criterion. For instance, for $M_{\rm BH} = 2.5\,M_\odot$, $h = 0.8$, and $\alpha = 0.15$ we found an average value of about 0.8 for τ.

Figure 3 illustrates the variation of X-ray luminosity with time for different sets of model parameters and for offset times of 50 s, 100 s, 200 s, and 300 s. These parameters are similar to those considered in Figure 1; to show the generality of our result, we extended the sets of parameters for the inset to include those regarded in Figure 4. Besides the fact that the power-law fit for L_p and t_p is in good agreement with phenomenological predictions, taking the magnetic barrier into account leads to an increase in the peak luminosity by an order of magnitude in comparison with similar cases for the zero-torque boundary condition. This is an expected result according to general relativistic magnetohydrodynamic simulations performed, e.g., by McKinney et al. (2012) and Tchekhovskoy et al. (2011).

Regarding Figure 4, our fits for the other two shape parameters k and w confirm a satisfactory robustness of our model in reproducing the shape of the light curve for the case of the zero-mass-flux boundary condition as well as the zero-torque boundary condition.

However, we must point out some issues on the subject of the magnetic barrier mechanism. On the one hand, Liu et al. (2014), through the study of a self-gravitating neutrino-dominated accretion disk (called NDAF), confirmed that instabilities appear in the outer parts and away from the equatorial plane. From a magnetic point of view, Shahamat & Abbassi (2017) probed for the possibility of fragmentation in a self-gravitating magnetized NDAF and also found it to be possible in the outer parts and away from the equatorial plane. Thus, we think that clumps might be thinner than what we expected from the vertical structure of the late-time advection-dominated central engine, that is, smaller values of the h parameter should be more worthy of consideration. As a consequence, clumps of smaller masses would be more likely to form. On the other hand, regarding α in its physically meaningful range, we found that the magnetic barrier is mainly plausible in the case of heaver clumps (with masses of the order of 0.4–0.8 $M_\odot$). Therefore, we think that such a limitation might make it lees likely for the magnetic barrier to govern the evolution of the generated clumps. Moreover, we considered ϕ to be of the order of 10^{-2}, which might be an overestimation for the late-time accumulated magnetic flux, since, as time passes and the accretion rate drops, both the clump's magnetic field and the accumulated magnetic flux decline. Such a drop in magnetic field, which is more likely for higher values of $t_{\rm off}$, might weaken the possibility of the magnetic barrier even more (see, e.g., McKinney et al. 2012 and references therein).

In the context of a power-law correlation between L_p and t_p, there are some points of importance to be noticed. We need to emphasize that the time dependence we considered to set our
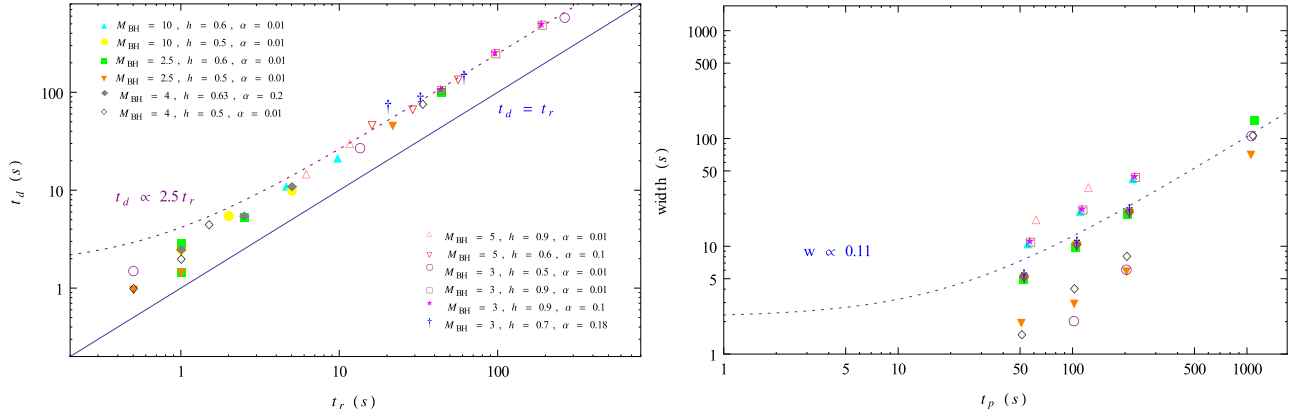
Figure 2. Left: decay time vs. rise time for various sets of model parameters and offset times with the linear fit as a dotted purple line. Right: best linear fit for the width parameter. Both fits show rather good agreement with observations, as discussed in the text. A zero-torque boundary condition has been considered.
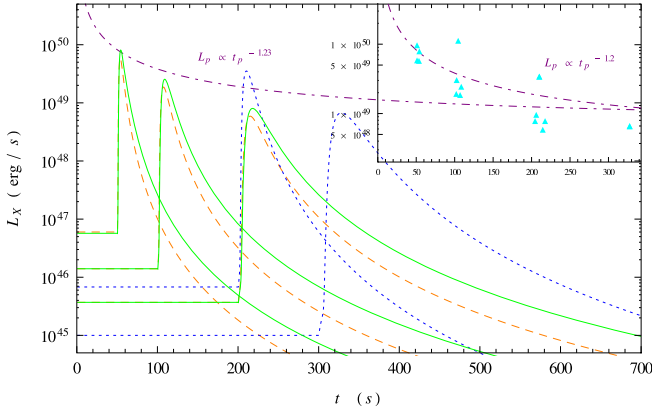
Figure 3. Same as Figure 1 in the case of the zero-flux boundary condition. Considering all sets of model parameters (those of Figure 4 have also been taken into account), the fit for the inner plot complies with observations as well as the other one (with only three sets of model parameters).

model parameters, such as the radius at which the clump is created, cannot lead to such a power-law behavior. This is because we have used these relations to apply some physically justified constraints to our model parameters, such as $\dot{M}$ and R_0, and these relations have not been applied directly in the time evolution equation of luminosity. In particular, Equation (21) has been used only to determine the accretion rate at $t_{\rm off}$ and it has not been considered in the main formalism of the model, which provides us with the time evolution of luminosity. In other words, we only aimed to use these relations to fix some model parameters regarding the offset time at which the clump starts to accrete. Hence, their time dependences have not influenced the clump's evolution directly, so that one can think of this power-law trend as a general outcome of our model.

4. Summary, Conclusions, and Discussion

We reconstructed the quantitative framework established by Dall'Osso et al. (2017), through a magnetic style in which small- and large-scale effects of magnetic field have been taken into account. To this end, we added one more term corresponding to the torque exerted by the Lorentz force (see Equation (5)). To solve this evolution equation, some approximations and assumptions have been implemented in

order to be able to adopt a similar semi-analytic approach to that proposed by Tanaka (2011) and followed by Dall'Osso et al. (2017). Through this method, we have provided final solutions that differ from those achieved by the previous work in some respects. First, for both cases of boundary conditions, the power-law dependence on radius changed in comparison with solutions obtained by Tanaka (2011). Second, considering h as an arbitrary parameter that is not just fixed at "1" (this affects $t_{\nu_{\rm in}}$ in the final solution) causes another difference in our result with respect to what has been achieved by Dall'Osso et al. (2017). Finally, to estimate model parameters such as clump mass, we limited ourselves to the correlations introduced between these parameters, so that our results are able to verify the framework we defined; however, in Dall'Osso et al. (2017) it was of less importance to consider such correlations in providing data. On the other hand, to investigate the possibility of a magnetic barrier occurring during each clump's viscous evolution, we compared the diffusion and viscous timescales. Moreover, two different boundary conditions have been imposed, i.e., zero torque and zero mass flux, in the hope of distinguishing the presence of the accumulated magnetic flux inside the inner regions, and consequently the magnetic barrier mechanism. We then studied the validity of our model through some key analogies to phenomenological findings. Our main conclusions can be identified as follows.

1. The ratio of width to peak time is found to be an almost constant, although somewhat scattered, parameter with an average value ~ 0.1, which is in rather good agreement with its phenomenological estimate, ~ 0.2. We also came to the conclusion that a magnetic barrier, if it exists, will not change this parameter significantly; instead, it might cause our data to become less scattered (left panel in Figure 4).

2. The insensitivity to model parameters of the skewness of the X-ray light curves (the asymmetry parameter) reveals another robust aspect of our model. This important feature is respected for both boundary conditions, with a similar value of about ~ 2.4, which is in satisfying agreement with its observational prediction, i.e., ~ 2.

3. Interestingly, the power-law correlation between the maximum value of luminosity and peak time, with a value of about ~ -1.3, is found to be close to what was estimated by Yi et al. (2016) from a phenomenological
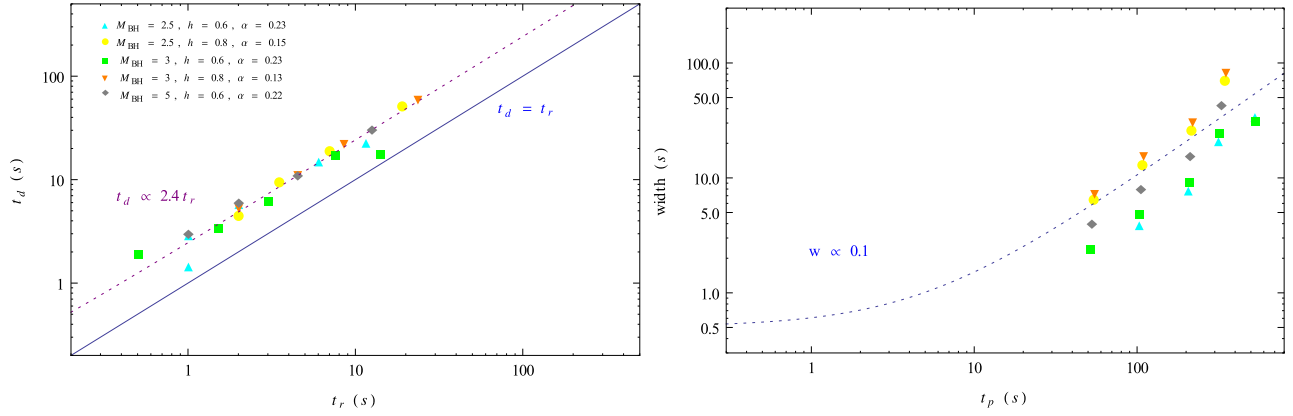
Figure 4. Fits for the asymmetry parameter (left) and the variation of width with peak time (right) where the zero-flux boundary condition has been taken into account.

point of view, i.e., ~-1.27. Both boundary conditions adopted here respect this feature.

There are some more points worth discussing here. For one thing, Dall'Osso et al. (2017) found the bolometric luminosity to be far from satisfactory in comparison with observations. However, after conducting a spectral correction through the adoption of a time-dependent X-ray efficiency, they modified the results to be well matched with observations. Whereas, considering the large-scale effect of a magnetic field led us to obtain shape parameters in close agreement with phenomenological values in both cases of bolometric and X-ray luminosities. Note that, in our study, bolometric luminosity differs from X-ray luminosity only by a constant coefficient, $L_X = f_X L_{bol}$. Thus, the bolometric and X-ray light curves have the same shape parameters in our model.

Another point is that we assumed f_{rad} and f_X to be constants. Accounting for any inconstancy about these two parameters might affect the shape of the light curve. On the one hand, simulations lead us to conclude that the efficiency in converting torus mass into jet energy varies from a few per cent up to more than 100%. The black hole spin, the disk thickness, and the magnetic flux might effectively alter this parameter (see, e.g., Giacomazzo et al. 2013 and references therein). On the other hand, regarding f_X, Dall'Osso et al. (2017) argued that a time-dependent X-ray efficiency with a decreasing trend in time (which is in agreement with the "curvature effect" if the emitting region has an accelerated bulk relativistic motion (Uhm & Zhang 2015, 2016)) might affect the spectral properties of X-ray flares.

Separate from these considerations, our simple model, together with the other probable modifications, could efficiently reproduce the spectral properties of X-ray flares. However, more precise studies via simulations appear to be essential to shed more light on the dark nature of the late-time evolution of a GRB's central engine.

Appendix A
Boundary Conditions and Green's Functions

Following Dall'Osso et al. (2017), to find the Green function, we adopted assumed the viscosity to follow a radial power law, $\nu \propto R^n$, and assumed a separable ansatz of the form $\Sigma(R, t) = R^p \sigma(R) e^{-\lambda t}$, where p and Λ are real numbers and σ is an arbitrary function of R, so that Equation (9) can be

rewritten as a Bessel differential equation (Tanaka 2011):

$$\frac{\partial^2 \sigma}{\partial R^2} + \frac{\partial \sigma}{R \partial R}(1.5 + 3/h + 2(n + p))$$
$$+ \sigma(R)\left[\frac{\Lambda}{3s}R^{-n} + \frac{(n + p)(0.5 + 3/h + (n + p))}{R^2}\right] = 0$$
(26)

where $s = \nu R^{-n}$ is a constant. It should be mentioned that we considered the Newtonian potential with $\Omega = \sqrt{GM/R^3}$. We also choose $p = n + \frac{1 - b_1}{2}$, with $b_1 = 1.5 + 3/h$, and $\Lambda = 3sk^2$. All these considerations, besides comparing Equation (26) with the transformed Bessel function

$$\frac{\partial^2 y}{\partial x^2} - \frac{\partial y}{\partial x}\left(\frac{2\alpha - 1}{x}\right) + y(x)\left[\frac{\alpha^2 - l^2\gamma^2}{x^2} + \beta^2\gamma^2 x^{2\gamma-2}\right]$$
$$= 0,$$
(27)

yield

$$\gamma = 1 - n/2; \ \ \beta = \frac{k}{1 - n/2}; \ \ \alpha = 2n; \ \ l = \frac{|1 - b_1|}{2(1 - n/2)}.$$

Now, the solution to Equation (10) can be written in the following form:

$$\sigma_k(R) = R^{-2n}[A(k)J_l(ky) + B(k)Y_l(ky)]$$
(28)

where $y = \frac{R^{1-n/2}}{1 - n/2}$. It is worth noting that in case of non-integer l, Y_l must be replaced by J_{-l}. Integrating the above solution over all possible k-modes gives the solution

$$\Sigma(R, t) = \int_0^\infty R^{-n-1/4}[A(k)J_l(ky) + B(k)Y_l(ky)]e^{-3sk^2t}dk.$$
(29)

The mode-weighting functions $A(k)$ and $B(k)$ are determined by the boundary conditions and the initial surface density profile $\Sigma(R, t = 0)$.

We just elaborate the zero-mass-flux boundary condition here, because the zero-torque one is implemented in a similar way. Before any further calculation to get the final solution, it is better to determine s in the power-law expression for viscosity as follows. The (magnetic) viscosity can be parameterized as $\nu = \alpha c_s^2/\Omega$ (Shakura & Sunyaev 1973; Pringle 1991). On the other hand, invoking hydrostatic

equilibrium perpendicular to the disk plane gives us $H = c_s/\Omega$, and consequently one can infer $\nu = \alpha h^2 \sqrt{GM} R^{1/2}$, which yields $s = \alpha h^2 \sqrt{GM}$ and $n = 1/2$. Furthermore, considering the continuity equation

$$R \frac{\partial \Sigma}{\partial t} + \frac{\partial \Sigma R v_R}{\partial R} = 0, \tag{30}$$

together with

$$\dot{M} = -2\pi \Sigma R v_R,$$

lead us to

$$\frac{\partial \Sigma}{\partial t} = \frac{1}{2\pi R} \frac{\partial \dot{M}}{\partial R}. \tag{31}$$

Comparing Equations (31) and (9) provides us with the following result:

$$\dot{M} \propto \left[\frac{\partial}{\partial R} \left(R^3 \nu \Sigma \frac{d\Omega}{dr} \right) + 3 \frac{d\Omega}{dR} \frac{\Sigma}{h} \nu R^2 \right] |_{R_{in}} = 0. \tag{32}$$

By substitution of the corresponding expressions for ν, Ω, and Σ, and making use of the recurrence relations between different Bessel functions

$$J_{l-1}(x) - J_{l+1}(x) = 2J_l'(x)$$

$$J_{l-1}(x) + J_{l+1}(x) = 2l \frac{J_l}{x}(x),$$

the following relation can be achieved:

$$\frac{A(\kappa)}{B(\kappa)} = -\frac{Y_{l-1}(\kappa)}{J_{l-1}(\kappa)}, \tag{33}$$

where $\kappa = k y_{in}$. As we proceed below, we need to obtain some more ingredients to get the final solution for $\Sigma(R, t)$. First,

$$\Lambda = 3sk^2 = 3\nu R^{-n} k^2,$$

and, second, we know

$$t_\nu = \frac{2}{3} \frac{R^2}{\nu} = \frac{2}{3} \frac{R^{2-n}}{s}. \tag{34}$$

Thus, Λ can be rewritten in the form

$$\Lambda = -2\kappa^2 (1 - n/2)^2 \frac{1}{t_{\nu_{in}}}.$$

Combining all the above, the expression for surface density takes the form

$$\Sigma = \int_0^\infty R^{-n+(1-b_1)/2} [c(\kappa)\kappa^{-1}][Y_{l-1}(\kappa)J_l(\kappa x) - Y_l(\kappa x)J_{l-1}(\kappa)] e^{-2\kappa^2 (1-n/2)^2 t/t_{\nu_{in}}} \kappa \, d\kappa$$

where $t_{\nu_{in}}$ is the viscous timescale of the inner radius of the disk and $x = y/y_{in}$. The mode weight $c(\kappa)$ might be obtainable by making use of a generalized Weber transform (Zhang et al. 2006;

Tanaka 2011)

$$\phi_l(x) = \int_0^\infty \frac{W_l(k, x; a, b)}{Q_l^2(k, ; a, b)} \Phi_l(\kappa) \kappa \, d\kappa$$

$$\Phi_l(\kappa) = \int_1^\infty W_l(\kappa, x; a, b) \phi_l(x) x \, dx$$

where

$$W_l = J_l(\kappa x)[(a - lb)Y_l(\kappa) + b\kappa Y_{l-1}(\kappa)] - Y_l(\kappa x)[(a - lb)J_l(\kappa) + b\kappa J_{l-1}(\kappa)]$$

and

$$Q_l^2 = [(a - lb)Y_l(\kappa) + b\kappa Y_{l-1}(\kappa)]^2 - [(a - lb)J_l(\kappa) + b\kappa J_{l-1}(\kappa)]^2.$$

If $a = 1$ and $b = 0$, the pair is identical to the ordinary Weber transform. However, $a = l$ and $b = 1$ correspond to our desired boundary condition, i.e., zero mass flux. After all, what would be the Green function? Clearly,

$$R^{n-(1-b_1)/2} \Sigma(R, t = 0) = \int_0^\infty [c(\kappa)\kappa^{-1}][Y_{l-1}(\kappa)J_l(\kappa x) - Y_l(\kappa x)J_{l-1}(\kappa)] \kappa \, d\kappa.$$

Finally, through applying the above considerations and running some more calculations, one may achieve the following result for $c(\kappa)$:

$$c(\kappa)$$
$$= \int_1^\infty \frac{R^{n-(1-b_1)/2} \Sigma(R, 0)[Y_{l-1}(\kappa)J_l(\kappa x) - Y_l(\kappa x)J_{l-1}(\kappa)]x \, dx}{[Y_{l-1}^2(\kappa) + J_{l-1}^2(\kappa)]}.$$

Thus,

$$\Sigma(R, t) = \int_0^\infty \left(\frac{\int_{r_{in}}^\infty [Y_{l-1}(\kappa)J_l(\kappa x') - Y_l(\kappa x')J_{l-1}(\kappa)] \Sigma(R', 0) \frac{(R')^{(1+b_1)/2}}{R_{in}^{2-n}} dR'}{[Y_{l-1}^2(\kappa) + J_{l-1}^2(\kappa)]} \right)$$
$$\times (1 - n/2) R^{-n+(1-b_1)/2} [Y_{l-1}(\kappa)J_l(\kappa x) - Y_l(\kappa x)J_{l-1}(\kappa)] e^{-2\kappa^2(1-n/2)^2 t/t_{\nu_{in}}} \kappa \, d\kappa.$$

Considering Equation (10), the Green's function would be obtainable as

$$G(R, R', t) = \int_0^\infty \frac{[Y_{l-1}(\kappa)J_l(\kappa x') - Y_l(\kappa x')J_{l-1}(\kappa)]}{[Y_{l-1}^2(\kappa) + J_{l-1}^2(\kappa)]}$$
$$\times \frac{(R')^{(1+b_1)/2}}{R_{in}^{2-n}} (1 - n/2) R^{-n+(1-b_1)/2}$$
$$\times [Y_{l-1}(\kappa)J_l(\kappa x) - Y_l(\kappa x)J_{l-1}(\kappa)]$$
$$\times e^{-2\kappa^2(1-n/2)^2 t/t_{\nu_{in}}} d\kappa. \tag{35}$$

Finally, regarding the initial surface density as

$$\Sigma(R, t = 0) = \Sigma_0 R_0 \delta(R - R_0) \tag{36}$$

in which Σ_0 and R_0 are arbitrary (Tanaka 2011), we have

$$\frac{\Sigma}{\Sigma_0} = \int_0^\infty \frac{R}{R_0}^{-n+(1-b_1)/2} \left(\frac{R_0}{R_{\rm in}}\right)^{2-n}$$
$$\times (1-n/2) e^{-2\kappa^2(1-n/2)^2 t/t_{\nu_{\rm in}}}$$
$$\times [Y_{l-1}(\kappa) J_l(\kappa x_0) - Y_l(\kappa x_0) J_{l-1}(\kappa)]$$
$$\times \frac{[Y_{l-1}(\kappa) J_l(\kappa x) - Y_l(\kappa x) J_{l-1}(\kappa)]}{[Y_{l-1}^2(\kappa) + J_{l-1}^2(\kappa)]} \kappa \, d\kappa \qquad (37)$$

Likewise, in the case of the zero-central-torque boundary condition, one can evaluate the Green's function as

$$G(R, R', t) = \int_0^\infty \frac{[Y_l(\kappa) J_l(\kappa x') - Y_l(\kappa x') J_l(\kappa)]}{[Y_l^2(\kappa) + J_l^2(\kappa)]}$$
$$\times \frac{(R')^{(1+b_1)/2}}{R_{\rm in}^{2-n}} (1-n/2) R^{-n+(1-b_1)/2}$$
$$\times [Y_l(\kappa) J_l(\kappa x) - Y_l(\kappa x) J_l(\kappa)]$$
$$\times e^{-2\kappa^2(1-n/2)^2 t/t_{\nu_{\rm in}}} \kappa \, d\kappa \qquad (38)$$

and subsequently the surface density will read

$$\frac{\Sigma}{\Sigma_0} = \int_0^\infty \frac{R}{R_0}^{-n+(1-b_1)/2} \left(\frac{R_0}{R_{\rm in}}\right)^{2-n}$$
$$\times (1-n/2) e^{-2\kappa^2(1-n/2)^2 t/t_{\nu_{\rm in}}}$$
$$\times [Y_l(\kappa) J_l(\kappa x_0) - Y_l(\kappa x_0) J_l(\kappa)]$$
$$\times \frac{[Y_l(\kappa) J_l(\kappa x) - Y_l(\kappa x) J_l(\kappa)]}{[Y_l^2(\kappa) + J_l^2(\kappa)]} \kappa \, d\kappa \qquad (39)$$

ORCID iDs

Shahram Abbassi ⓘ https://orcid.org/0000-0003-0428-2140

References

Beniamini, P., & Kumar, P. 2016, MNRAS, 457, L108
Binney, J., & Tremaine, S. 1987, Galactic Dynamics (Princeton: Princeton Univ. Press)
Blandford, R. D., & Znajek, R. L. 1977, MNRAS, 179, 433
Burrows, D. N., Romano, P., Falcone, A., et al. 2005, Sci, 309, 1833
Campana, S., Tagliaferri, G., Lazzati, D., et al. 2006, A&A, 454, 113
Chincarini, G., Mao, J., Margutti, R., et al. 2010, MNRAS, 406, 2113
Chincarini, G., Moretti, A., Romano, P., et al. 2007, ApJ, 671, 1903
Cusumano, G., Mangano, V., Chincarini, G., et al. 2006, Natur, 440, 164
Dai, Z. G., Wang, X. Y., Wu, X. F., & Zhang, B. 2006, Sci, 311, 1127
Dall'Osso, S. D., Perna, R., Tanaka, T. L., & Margutti, R. 2017, MNRAS, 464, 4399
D'Angelo, C. R., & Spruit, H. C. 2010, MNRAS, 406, 1208
D'Angelo, C. R., & Spruit, H. C. 2011, MNRAS, 416, 893
D'Angelo, C. R., & Spruit, H. C. 2012, MNRAS, 420, 416
Falcone, A. D., Burrows, D. N., Lazzati, D., et al. 2006, ApJ, 641, 1010
Fan, Y. Z., & Piran, T. 2006, MNRAS, 369, 197
Fragile, P. C., Wilson, J., & Rodriguez, M. 2012, MNRAS, 424, 524
Gammie, C. F. 2001, ApJ, 553, 174
Giacomazzo, B., Perna, R., Rezzolla, L., Troja, E., & Lazzati, D. 2013, ApJ, 762L, 18
Guidorzi, C., Dichiara, S., Frontera, F., et al. 2015, ApJ, 801, 57
Ioka, K., Kobayashi, S., & Zhang, B. 2005, ApJ, 631, 429
Jin, Z. P., Fan, Y. Z., & Wei, D. M. 2010, ApJ, 724, 861
Kato, S., Fukue, J., & Mineshige, S. 2008, Black Hole Accretion Disks: Toward a New Paradigm (Kyoto: Kyoto Univ. Press)
King, A., O'Brien, P. T., Goad, M. R., et al. 2005, ApJL, 630, L113
Lazzati, D., & Perna, R. 2007, MNRAS, 375, 46
Lee, H. K., Wijers, R. A. M. J., & Brown, G. E. 2000, PhR, 325, 83
Liu, T., Yu, X. F., Gu, W. M., & Lu, J. F. 2014, ApJ, 791, 69
Lloyd-Ronning, N. M., Dolence, J. C., & Fryer, C. L. 2016, MNRAS, 461, 1045
Lynden-Bell, D., & Pringle, J. E. 1974, MNRAS, 168, 603
Margutti, R., Bernardini, G., Barniol Duran, R., et al. 2011, MNRAS, 410, 1064
Margutti, R., Guidorzi, C., Chincarini, G., et al. 2010, MNRAS, 406, 2149
McKinney, J. C., Tchekhovskoy, A., & Blandford, R. D. 2012, MNRAS, 423, 3083
Meszaros, P., & Rees, M. J. 1997, ApJ, 476, 232
Metzger, B. D., Piro, A. L., Tanaka, T. L., & Quataert, E. 2008, MNRAS, 390, 781
Narayan, R., Igumenshchev, I. V., & Abramowicz, M. A. 2003, PASJ, 55, L69
Nousek, J. A., Kouveliotou, C., Grupe, D., et al. 2006, ApJ, 642, 389
O'Brien, P. T., Willingale, R., Osborne, J., et al. 2006, ApJ, 647, 1213
Perna, R., Armitage, P. J., & Zhang, B. 2006, ApJL, 636, L29
Pringle, J. E. 1991, MNRAS, 248, 754
Proga, D., & Zhang, B. 2006, MNRAS, 370L, 61
Romano, P., Moretti, A., Banat, P. L., et al. 2006, A&A, 450, 59
Shahamat, N., & Abbassi, S. 2017, ApJ, 845, 64
Shakura, N. I., & Sunyaev, R. A. 1973, A&A, 24, 337
Shu, F. H. 1992, The Physics of Astrophysics, Vol. 2 (Mill Valley, CA: Univ. Science Books)
Takeuchi, T., Miyama, S. M., & Lin, D. N. C. 1996, ApJ, 460, 832
Tanaka, T. 2011, MNRAS, 410, 1007
Tanaka, T. L. 2013, MNRAS, 434, 2275
Tchekhovskoy, A., Narayan, R., & McKinney, J. C. 2011, MNRAS, 418, L79
Toomre, A. 1964, ApJ, 139, 1217
Uhm, Z. L., & Zhang, B. 2015, ApJ, 808, 33
Uhm, Z. L., & Zhang, B. 2016, ApJL, 824, L16
Xie, Y., Huang, Z. Y., Jia, X. F., Fan, S. J., & Liu, F. F. 2009, MNRAS, 398, 583
Yi, S. X., Xi, S. Q., Yu, H., et al. 2016, ApJS, 224, 20
Zhang, B., Fan, Y. Z., Dyks, J., et al. 2006, ApJ, 642, 354